

**DEVELOPMENT OF IMAGE PROCESSING
FOR RAPID NUMERICAL PHANTOM RECONSTRUCTION
AND MONTE CARLO CALCULATION FOR CALIBRATION
OF *IN VIVO* MEASUREMENT SYSTEMS**

N. Borisov, D. Franck, L. Laval, L. de Carlan

Institut de Protection et de Sûreté Nucléaire,
rue Auguste Lemaire, B.P. 6 – 92265 Fontenay-aux-Roses Cedex, France,
e-mail : nikolai_borissov@ipsn.fr, didier.franck@ipsn.fr

ABSTRACT

The paper reports on development of numeric phantoms for Monte Carlo calculations for *in vivo* measurements of radionuclides deposited in tissues. The individual properties of each person require rather precise geometric representations. It is particularly important for low energy gamma ray emitting sources as thorium, uranium, plutonium and other actinides. The new utility that allows automatic creation of MCNP initial file from individual scanning information, was developed. It includes segmentation of voxel matrix, obtained with both computerized tomography (CT) and magnetic resonance imaging (MRI), for distinguishing tissues by level of brightness, association colors with certain tissues, source and detector specification and, finally, voxel coupling to reduce the consumed memory and increase speed of calculations. The developed procedure was tested for low energy emitters, both on plastic and real biological tissues measurements, as well as for CT and MRI scanning information for MCNP input files.

1. INTRODUCTION

Although great efforts have been made to improve the physical phantoms used to calibrate *in vivo* measurement systems, these phantoms represent a single average counting geometry and usually contain a uniform distribution of the radionuclide over the tissue substitute. As a matter of fact, significant corrections must be made to phantom-based calibration factors in order to obtain absolute calibration efficiencies applicable to a given individual. The importance of these corrections is particularly crucial by considering *in vivo* measurements of low energy photon emitting radionuclides deposited in the lung such as actinides. Thus, it is desirable to develop a method for calibrating *in vivo* measurement systems that is more sensitive to these types of variability.

The crucial point is to use individual scanning data for creating a person-specified numerical phantom which will be both adequately representing the body structure and allowing three-dimensional transport calculations. Such calculations in real geometry without any restrictions can be done practically only with Monte Carlo method which is rather time-consuming. Previous works [1-6] have demonstrated the possibility of such a calibration using the Monte Carlo technique. Unfortunately, they use either rough resolution images for numeric phantoms due to memory capacity and calculation speed

restrictions [1-4], or simplified Monte Carlo codes rather than highly developed codes as MCNP [5-6]. Moreover, all of them use only static or statistically averaged scanning data and are not designed to treat universally the arbitrary geometry of an individual, which might not be sufficient for low-energy gamma contamination or special case such as wound contamination.

2. MCNP PHANTOM RECONSTRUCTION UTILITY

The presented research program extended such investigations to the reconstruction of numeric adequate anthropomorphic phantoms with the highest possible resolution based on personal physiological data. For automatization of preparation process for initial MCNP file, a special utility named “Anthropo” based in PV-Wave[®] visual data analysis system, is developed. It can be run both on Intel[®] and DEC Alpha[®] platforms under MS Windows[®] and UNIX systems respectively.

2.1 “Anthropo” interface functionality

The interface is specially designed for the data required for MCNP4b [7] to enable correct simulation of the photon spectra in the detectors generally used in gamma spectrometry and *in vivo* measurement system laboratories.

The “Anthropo” interface input data is of three orders: (i) magnetic resonance or scanned images of different sections of a phantom or a person, (ii) source description, i.e. the type of source (point or diffuse), the number of gamma-radiation lines used, their energy, their probability and the activity of the sources, making it possible to directly calculate the number of histories used in the simulation with MCNP4b and finally, (iii) the geometry of the detector and its positioning relative to the numerical phantom.

To facilitate MCNP file creation and processing, specials modules are created for saving, and for image processing and display. The latter are first used for segmenting the images on the basis of the different levels of gray obtained when creating images by tomography or magnetic resonance (Figure 1), and then for associating different organs with the tissues specified by the ICRU-44 report [8]. The MCNP4b code input file is then automatically written by the “Anthropo” interface. It consists of the above data plus data relating to the geometry of the detector and the materials it is made of, the nature of the sources and finally the quantities required from the calculations (referred to as the “tally” in the MCNP code), i.e. in our case, the spectrum of the energy deposited in the counter. This stage is completely automatic. To check that the MCNP4b input file is properly configured, the overall geometry (phantom + detector) is displayed using the Sabrina code [9].

After MCNP calculation, the output MCNP file as well as output file of experimental protocol can be loaded for graphic comparison of calculated and experimental spectra.

2.2 Segmentation of the image

The very crucial point in association of voxel with certain tissues is the segmentation process. In the developed utility, this process can follow the possible decreasing resolution of the image and cutting margins of each slide, which can contain several artifacts (especially for MRI images, which contain sufficient irregularities on the sides, where magnetic field strength is very high that cause to different artifacts). The segmentation itself does distinguish tissue from tissue by brightness level for given level boundaries, improve the homogeneity of segmented image with erosion and dilatation procedures and, finally, associate colors with tissues.

For CT images the segmentation process is shown on fig. 1 for the anthropomorphic Livermore phantom specially developed for calibration of lung monitoring facilities [10]. The upper left window represents slices of the original CT image, the lower left window — of the segmented image with several large areas with uniform color. The histogram at upper right corner shows the brightness profile of current slide, clearly showing peaks corresponding to bones, lungs, soft tissues and external air.

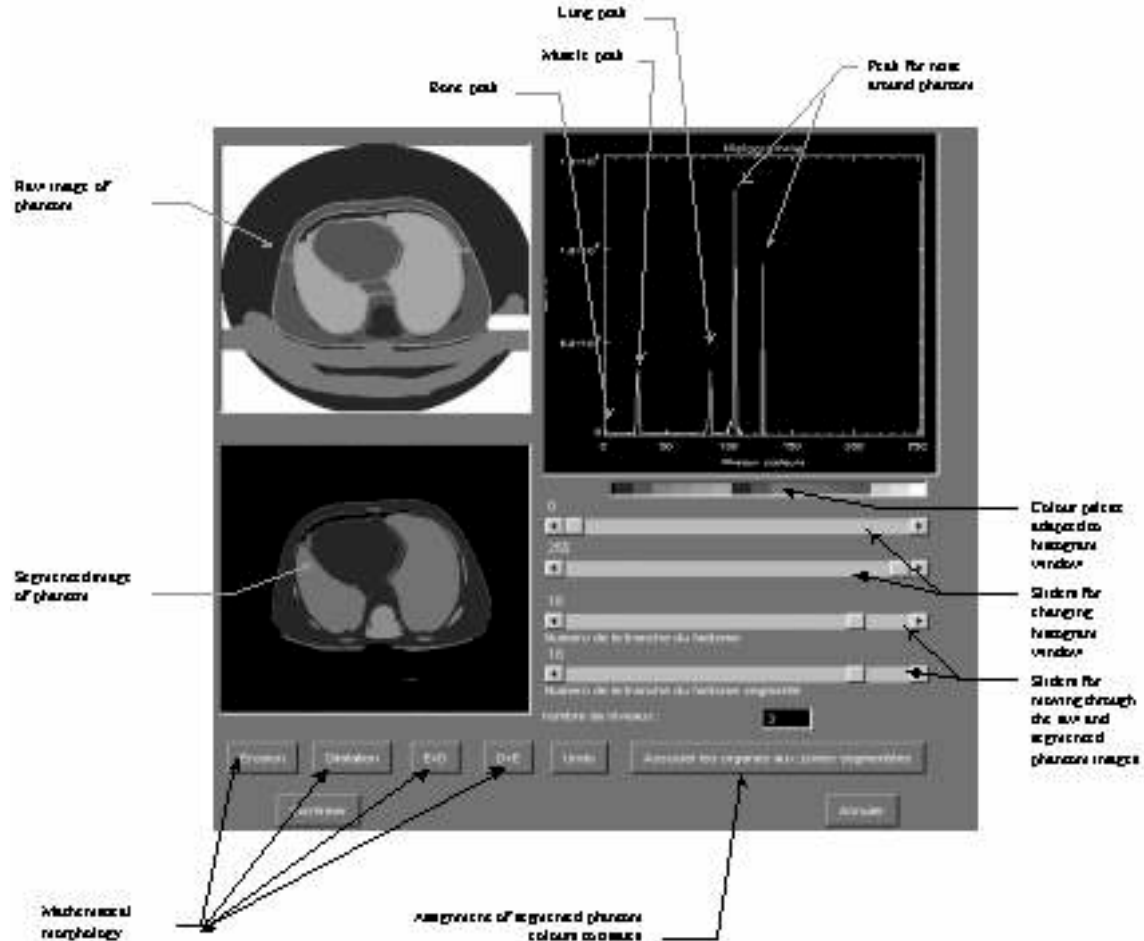


Fig. 1 Upper left window — original CT image, lower left window — segmented image. Histogram at upper right corner — brightness profile of current slice.

For MRI the problem of segmentation is not so trivial. MRI produces approximately equal brightness for significantly different tissues. The left part of fig. 2 illustrates this difficulty. After segmentation marginal parts of lungs are colored with the same color as fat, but the central part is colored with the same color as external air. To overcome such difficulties, the procedure of color correction is involved. After the same process as CT images shown on fig. 1, the user can change the color of the isolated solid, which contains the clicked voxel, or (optionally) change the color of all the voxel with the clicked color to new value. The algorithm of changing color for the isolated 3-D solid searches iteratively all the voxels with old color neighboring to voxels with changed color in subsequently extended boundaries of the solid and changes the color of such neighbors until no new neighbor is found. After it the algorithm checks for the neighbors inside the rectangular area containing new boundaries of the solid. Then it returns to extend the boundaries again and check for the new possible neighbor voxels. If two subsequent searches (on the boundaries and inside them) produce no neighboring voxels, the search is terminated. Analogous algorithm was developed for two-dimensional search (within one slice).

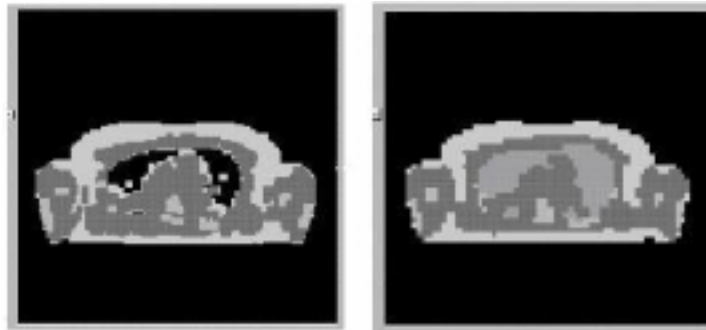


Fig. 2 Images before and after color correction.
After segmentation some parts of lungs are colored with different colors,
after correction they were repainted with the new color.

The example of gradual progress of two-dimensional color correction algorithm for Livermore phantom image is shown on fig. 3. The muscle tissue color is changed from black to white. The dark spot in right lower corner of the first image represent the trace of the mouse, used to point to the initial voxel. The results of color change are given in the right part of fig. 2. Lung tissues were successfully distinguished and associated with proper color.

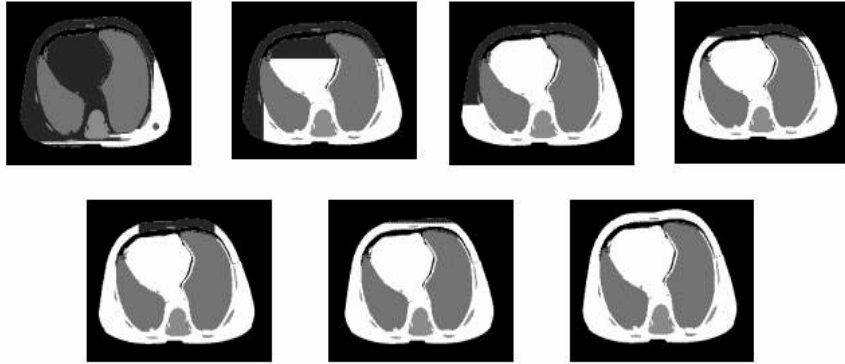


Fig 3. Steps of color correction algorithm. Muscle tissue color is changed from black to white from the voxel marked with black spot.

3.2 Source and detector specification

In order to simulate the geometry of measurements, the utility can specify sources (both point and distributed through the tissue, on the user's choice). The user can choose either a certain nuclide from the menu shown in upper figure, or compose the custom set of energies and quantum release factors. It is possible to specify a mixed-nuclide, such as MOX, contamination, defining the activity or mass composition of the nuclides.

The certain type of detector with previously defined geometry, provided by the manufacturer, can also can be specified the proper detector (now three types of germanium detectors and one type of silicon detector are involved). After choosing the detector can be placed to proper position and orientation.

3.2MCNP initial file creation

The data can be written as initial MCNP file to calculate pulse-height-spectrum in the detector. This procedure includes processing of information on the voxel phantom, source, detector and calibration of spectrometry channels. To take advantage of high-resolution images, the procedure of coupling the neighboring voxels with the same density and material to unitary MCNP cells is developed. For internal MCNP reason, the calculation speed depends on the number of cells described with intersection ('AND') procedure. That means than one shouldn't minimize the number of logical cells, coupling cells into concave solids with junction ('OR') procedure. The only type of the solid, which can be described with intersection in MCNP geometry if using only planar surfaces, which are perpendicular to Cartesian axes, is rectangular box. It means that, to reduce the computation time, one should express the phantom as sum of rectangular boxes. To construct coupled boxes, a special algorithm is developed.

The algorithm of 3-D voxel coupling is based upon extension of new box in three dimensions simultaneously until any concavity with another tissue is found. Then it

checks if it is possible to extend the box further simultaneously in two dimensions (the priority hierarchy of extension x , y , z subsequently). When extension in two dimensions becomes impossible, the algorithm checks, if further one-dimensional extension can be done (the axis priority hierarchy is the same). The extension terminates when every one-dimensional movement is impossible. The procedure of one-dimensional coupling, in which only neighbors along one axis can be coupled, is also possible. The difference between coupled and non-coupled cell representation of Sabrina[®] visualized MCNP file is shown on fig. 4. Different colors represent different cells.



Fig. 4 Voxel coupling. From left to right: no coupling, one-dimensional coupling and three-dimensional coupling. Different colors represent different cells.

3. VALIDATION OF THE UTILITY

The new utility was, described in the previous chapter; was tested on examples of reconstruction of both low- and high-resolution MCNP phantoms for whole body counting of low-energy gamma rays on base of both CT and MRI scanning images.

3.1 Voxel coupling algorithm

As an example, a CT image tomography of Livermore plastic chest phantom was used. Several step of MCNP input file creation are discussed in the previous section. The advantage of voxel coupling procedure is shown in tab. 1, which first row (N_C) of each cell contains the comparison of number of cells both for rough ($32 \times 32 \times 17$ voxels) and realistically high ($128 \times 128 \times 40$ voxels) resolution phantoms is done. The number of cells for high resolution without voxel coupling is about 200,000 and any calculations are practically impossible due many days required to obtain the acceptable accuracy. The second row (T_{DA}) of each cell contains the data on required computation time for one random story produced by lung source for DEC Alpha[®] professional workstation (frequency 1 GHz, memory 512 Mb), and the third row (T_{PC}) — for Intel[®] Pentium[®] III PC (frequency 400 MHz, memory 64 Mb). Voxel coupling reduces number of cells and computation time more than by an order. This advantage is more essential for distributed source calculation, when the computation time for high-resolution phantom and even coupled voxel cells takes a day or more.

Table 1 From up to down: Number of cells (N_C), computation time for one random with story with DEC Alpha[®] workstation (T_{DA}), and Intel[®] Pentium[®] III PC (T_{PC}) for ²⁴¹Am lung source, 10⁻⁶ min

Resolution		No coupling	1-D coupling	3-D coupling
Rough	N_C	6468	1466	448
	T_{DA}	157	36	15
	T_{PC}	484	111	45
High	N_C	≅200,000	11389	4437
	T_{DA}	—	282	107
	T_{PC}	—	887	330

The comparison of calculated spectrum with experimentally measured for uniform lung contamination of 70 kBq of ²⁴¹Am is shown in fig. 5. Experimental data show the good consistence with simulation both in full absorption peak of the most powerful ²⁴¹Am line and in Compton scattering area. The achieved standard deviation in the spectrometric channel with maximal intensity is about 3% for 2h30min calculation. The difference between absolute value of full absorption peak intensity for measurement and MCNP calculations is about only 10%, which can be explained due to geometric uncertainty, which means that no special efficiency correction for calibration is required.

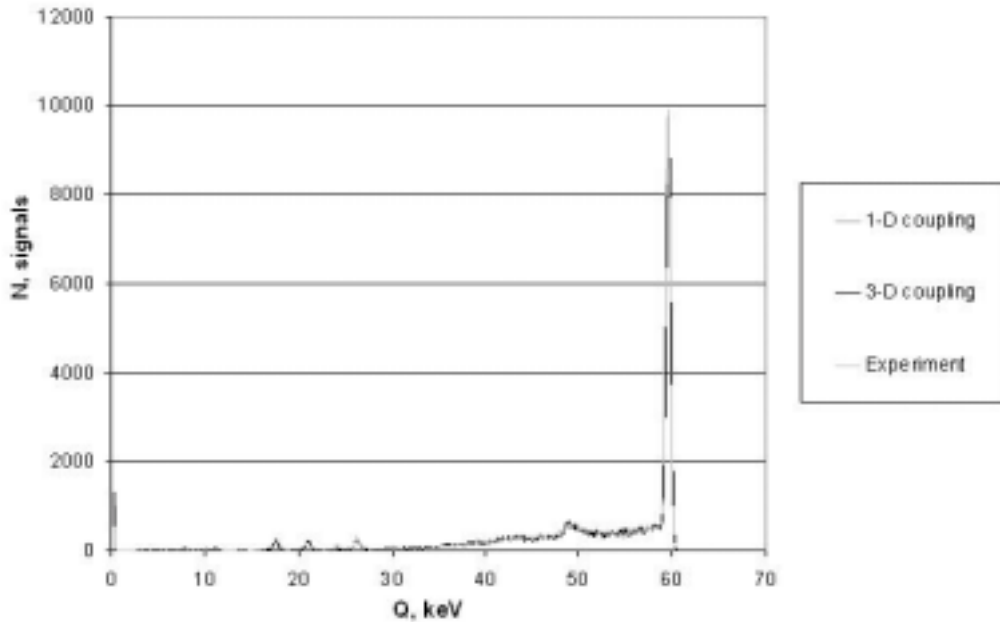


Fig. 5 Comparison of experimental and MCNP pulse-height-spectrum from lung ²⁴¹Am contamination.

3.2 Use of personal MRI image for MCNP phantoms

To validate the ability of the system to use personal MRI images for MCNP phantom creation and measurement calibration, several experiments with arbitrary samples of biologic tissues (meat) were conducted. The sample geometries were scanned at MRI scanning device “MAGNETOM EXPERT plus H-SP-CR VB33D” at Hôpital d’Instruction des Armées, Percy (see fig. 6, on the left). After scanning, point etalon radionuclide sources (for example, 32 kBq of ^{241}Am) were put into the depth of the sample and provided measurements on the high purity germanium gamma-spectrometer “Canberra Semiconductors NV”(see fig. 6, on the right).

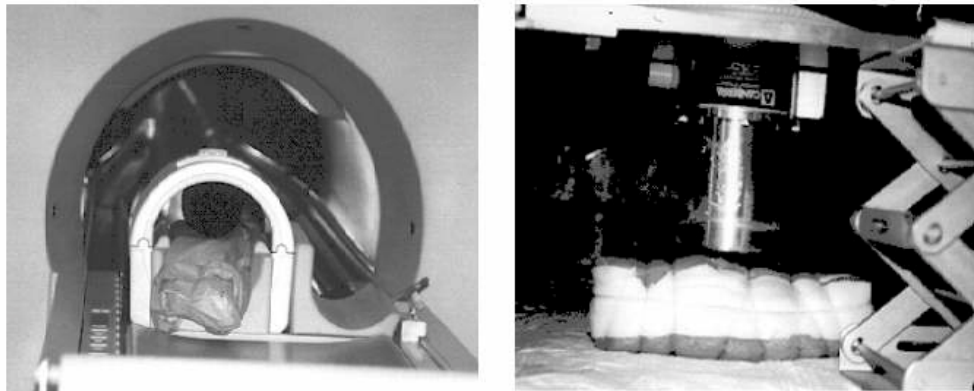


Fig. 6 Experimental validation of MRI processing algorithm. On the left — scanning the meat sample on MRI device “MAGNETOM EXPERT plus H-SP-CR VB33D” at Hôpital d’Instruction des Armées, Percy. On the right — spectrometry measurement with meat samples at germanium gamma- spectrometer “Canberra Semiconductors NV”.

The absolute pulse-height-spectra for three one of meat sample (mouton knee), visualized with “Anthropo” utility, are shown at figure 7. To the right from the spectrum, the photograph image of the sample and Sabrina[®] visualization of MCNP initial file (sample with the detector) are shown. The brighter line indicates MCNP results, the darker — experimental. Within the experimental error the full absorption peak intensity are similar for measurement and calculation for all the geometries, including described in the previous section Livermore chest phantom geometry, as it is shown in the table 2. Due to uncertainty of the exact place of the source inside the samples, it was rather difficult to compare accurately the efficiency of registration. This uncertainty is particularly essential for the chicken sample, where the source was placed inside the body cavity and not fixed inside. The calculation time for DEC Alpha[®] station and 3-D voxel coupling depends on the complexity of the geometry. To achieve 1.5%-2% for the standard deviation in the maximum spectrometry channel, which is possible after one million of statistic histories, one should spend from 3min30s (beef sample) up to 17min20s (chicken sample).

Table 2 Full absorption peak intensity for measurement and calculation, signals/sec

Geometry	Plastic chest Livermore phantom, lung ^{241}Am source 70 kBq	Mouton knee, point ^{241}Am source 32 kBq	Chicken, point ^{241}Am source 32 kBq	Beef, point ^{241}Am source 32 kBq
Calculated	46	208	187	568
Measured	50	228	132	525
Difference, %	-8	-9	+40	+8

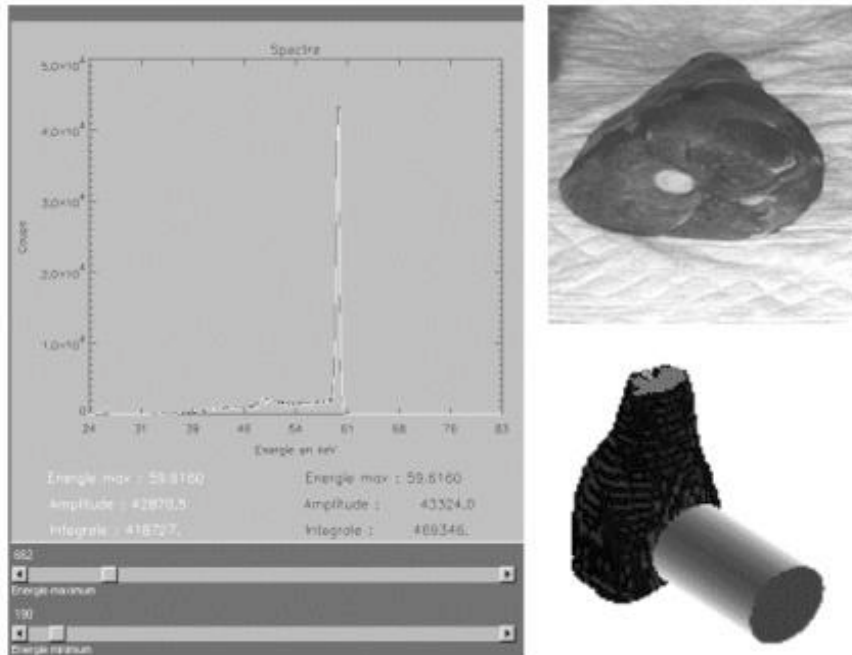


Fig. 7 Comparison with “Anthropo” utility of experimental and MCNP pulse-height-spectra from point ^{241}Am source, placed into mouton meat samples. On the right — photo image of the sample and Sabrina[®] visualization of MCNP geometry.

4. CONCLUSION AND PROSPECTIVES

Calibration using voxelized numerical phantoms with Monte Carlo calculations has already been suggested for solving *in vivo* measurement system X-ray and gamma ray spectrometry calibration problems. It has accordingly been demonstrated that this approach has considerable potential for the calibration of *in vivo* counting systems for measuring low energy x-ray and gamma ray emitters in the lung. The work described in this document was carried out with a view to extending use of this principle to the reconstruction of numerical phantoms based on physiological data relating to individuals to be measured, using magnetic resonance and scanner images.

The interface designed makes it possible to automatically create a MCNP4b computer code input file with complex three-dimensional phantom geometry reconstituted from images. It is realized in PV-Wave[®] Visual Data Analysis media for platform-independent (both UNIX and MS Windows[®]) use. It allows treatment of both MRI and X-ray CT images and could be used to prepare a realistic high-resolution phantom, which, however, requires achievable time for MCNP calculation with acceptable precision. The use of the utility is tested on reconstruction of MCNP phantoms for low-energy gamma ray counter calibration with arbitrary samples of biological material. The comparison of MCNP calculation and experimental results for reconstructed phantoms confirms that the utility is able to use properly arbitrary medical images for its purposes.

Consequently, as a result of its flexibility in accommodating complex geometry, the method developed not only represents a diagnostic tool for *in vivo* measurement, but also opens up new possibilities such as the optimization of detection systems, the study of contamination with mixed actinides and any other simulation using MCNP4b where complex geometry is derived from a set of superimposed images. This is particularly important not for only whole body counting application, but for other medical application such as dosimetry calculations for personally specified scanning data.

ACKNOWLEDGEMENTS

The authors acknowledge the assistance of Medical Imaging Service of Hôpital d'Instruction des Armées at Percy, Clamart and its head, Dr. D. Jeanbourquin, who gratefully provided all the MRI scanning of meat samples at the device "MAGNETOM EXPERT plus H-SP-CR VB33D".

REFERENCES

1. M. W. Mallet, D. P. Hickmann, D. A. Kruchten, J. W. Poston. Development of a Method for Calibrating *in vivo* Measurement Systems Using Magnetic Resonance Imaging and Monte Carlo Calculations. *Health Phys.*, **68**, pp. 773 — 785 (1995).
2. T. Ishikawa, M. Matsumoto, M. Uchiyama. A Calibration Method for Whole-Body Counters, Using Monte Carlo Simulation. **64**, pp. 283 — 288 (1996).
3. T. Ishikawa, M. Uchiyama. Calculation of the Counting Efficiency for ¹³⁷Cs Using Voxel phantom with Lungs and a Skeleton. *Radiat. Prot. Dosim.*, **69**, pp. 199 — 204 (1997).
4. T. Ishikawa, M. Uchiyama. Estimation of the Counting Efficiencies for Individual Subjects in ¹³⁷Cs Whole-Body Counting, Using Voxel Phantoms, *Radiat. Prot. Dosim.*, **71**, pp. 195 — 200 (1997).
5. J. G. Hunt, I. Malatova, S. Foltanova. Calculation and Measurement of Calibration Factors for Bone Surface Seeking Low Energy Gamma Emitters and

- Determination of ^{241}Am Activity in a Real Case of Internal Contamination. *Radiat. Prot. Dosim.*, **82**, pp. 215 — 218 (1998).
6. J. G. Hunt, I. Malatova, S. Foltanova, B. M. Dantas. Calibration of *In Vivo* Measurement System Using a Voxel Phantom. And the Monte Carlo Technique. *Radiat. Prot. Dosim.*, **89**, pp. 283 — 286 (2000).
 7. J. F. Briesmeister. MCNP-A General Monte Carlo N-Particle Transport Code, Version 4B. *LANL Memorandum*. Los Alamos National Laboratory. (1997).
 8. ICRU. Tissue Substitutes in Radiation Dosimetry and Measurements. ICRU Report 44. ICRU Publication, Bethesda. (1989).
 9. A.V. Kenneth. User's Guide for Sabrina[®]. Version 3.56, Radiation Transport Group – Applied Theoretical Physics Division – Los Alamos National Laboratory, LA-UR-93-3696. (1994).
 10. R. V. Griffith, P. N. Dean, A. L. Anderson, J. C. Fisher, A Tissue-Equivalent Torso Phantom for Intercalibration of *in vivo* Transuranic Nuclide Counting Facilities. In: *Advances in Radiation Protection Monitoring (Proc. Symp. Stockholm, 1978)*, IAEA 445, pp 493 – 504 (1979).